

RSC Advances



This is an *Accepted Manuscript*, which has been through the Royal Society of Chemistry peer review process and has been accepted for publication.

Accepted Manuscripts are published online shortly after acceptance, before technical editing, formatting and proof reading. Using this free service, authors can make their results available to the community, in citable form, before we publish the edited article. This *Accepted Manuscript* will be replaced by the edited, formatted and paginated article as soon as this is available.

You can find more information about *Accepted Manuscripts* in the [Information for Authors](#).

Please note that technical editing may introduce minor changes to the text and/or graphics, which may alter content. The journal's standard [Terms & Conditions](#) and the [Ethical guidelines](#) still apply. In no event shall the Royal Society of Chemistry be held responsible for any errors or omissions in this *Accepted Manuscript* or any consequences arising from the use of any information it contains.



Journal Name

ARTICLE

Stripe distributions of graphene-coated Cu foils and their effects on the reduction of graphene wrinkles

Haoran Zhang^{a,b}, Yanhui Zhang^a, Bin Wang^{a,c}, Zhiying Chen^a, Yaqian Zhang^{a,b}, Yanping Sui^a, Guanghui Yu^{a,*}, Zhi Jin^d, and Xinyu Liu^d

Received 00th January 20xx,
Accepted 00th January 20xx

DOI: 10.1039/x0xx00000x

www.rsc.org/

Hexagonal single-crystal domains of graphene were analyzed and the wrinkle distribution was obtained using thermal hydrogen etching. We observe parallel stripes on some single-crystal domains and these stripes are associated with graphene wrinkles. The etched trenches in graphene are always perpendicular to the stripes, thereby suggesting the suppressed formation of wrinkles along the stripe direction. Results indicate that the stripes help release the internal stress of graphene to reduce its wrinkle density. Furthermore, these stripes are due to Cu surface reconstruction and relate to two main factors, namely, the distribution of Cu grains and the cooling rate after graphene growth. Continuous graphene films which is synthesized by slow cooling exhibit high stripe area coverage and low sheet resistance because of the low wrinkle density.

Introduction

Graphene is a two-dimensional atomic layer of sp²-hybridized carbon atoms. This material is gaining substantial attention because of its distinct band structure and physical properties¹. Graphene grown on Cu foils by chemical vapor deposition (CVD) has been studied because of its cost efficiency and large monolayer coverage²⁻⁴. The mechanisms underlying graphene growth on Cu via CVD were determined⁵. Previous studies have focused on graphene nucleation^{6, 7}, growth rate⁸, and domain shape⁹⁻¹¹. CVD graphene often exhibits inferior electrical properties compared with exfoliated graphene^{2, 12} because of their boundaries¹³, defects^{12, 14}, and wrinkles¹⁵. The grain size has been increased to avoid the adverse effects of the boundaries of the graphene domain and improve the film quality. When the size of CVD graphene domains achieves the millimeter scale^{11, 16-18}, the density of the domain boundaries on the CVD graphene reduces and results in a weakened impact of graphene boundaries on graphene properties. Graphene wrinkles can cause relatively low

transport mobility in CVD graphene. Therefore, the wrinkles in graphene should be importantly removed.

Graphite has a negative thermal expansion coefficient in the temperature range of 0-700K¹⁹. The thermal expansion coefficient of single-layer graphene is strongly dependent on temperature and sometimes it is even negative ($-4.8 \times 10^{-6} \text{K}^{-1}$ in the range 0-300K reported by Zakharchenko *et al.*²⁰, $-8.0 \times 10^{-6} \text{K}^{-1}$ at room temperature by Yoon *et al.*²¹). Mismatches of the thermal expansion coefficient between graphene and Cu substrate ($17.5 \times 10^{-6} \text{K}^{-1}$) expand the graphene lattice and shrink Cu during cooling, thereby increasing the internal stress in graphene. The internal stress of graphene causes wrinkle formation^{22, 23}. Parallel stripes (height, approximately 1Å) have been induced by the stress and observed by scanning tunneling microscopy (STM)²⁴. Moreover, these stripes undergo thermal strain engineering on graphene flakes grown on liquid Cu surface²⁵. However, none of these studies have investigated the association of the stripes with graphene wrinkles. In this study, we find these stripes (height, 5 nm to 100 nm) are caused by Cu surface reconstruction (CSR) and associated with graphene wrinkles. Noting that the graphene wrinkles were indeed graphene ridges while the stripes were wrinkles in papers on surface instabilities²⁶. However, such definitions were inconsistent with the expressions in most literatures for graphene. Here, we defined the periodic surface structures as "stripes" and the high ridges as "wrinkles" in this text, corresponding to the previous literatures for graphene.

Hydrogen etching can be used to reveal the wrinkle distribution²⁷. High-resolution microscopic techniques, such as atomic force microscopy (AFM), scanning electron microscopy (SEM), and STM²² have been utilized to analyze the morphology of the wrinkles. However, large-scale information on the distribution and density of wrinkles is difficult to obtain

^aState Key Laboratory of Functional Materials for Informatics, Shanghai Institute of Microsystem and Information Technology, Chinese Academy of Sciences, 865 Changning Road, Shanghai 200050, China

^bUniversity of Chinese Academy of Sciences, No.19A Yuquan Road, Beijing 100049, China.

^cSchool of Physics and Optoelectronic Technology, Dalian University of Technology, 2 Linggong Road, Dalian 116024, China

^dMicrowave Devices and Integrated Circuits Department, Institute of Microelectronics, Chinese Academy of Sciences, 3 West Beitucheng Road, Beijing 100029, China

*Corresponding author. Tel: +86 21 62511070 8306.

E-mail address: ghyu@mail.sim.ac.cn (G. H. Yu).

Electronic Supplementary Information (ESI) available: [AFM images of CSR stripes, relationship between CSR stripes and etched trenches, optical images of transferred etched domains, Cu rugged structure and partial CSR stripes]. See DOI: 10.1039/x0xx00000x

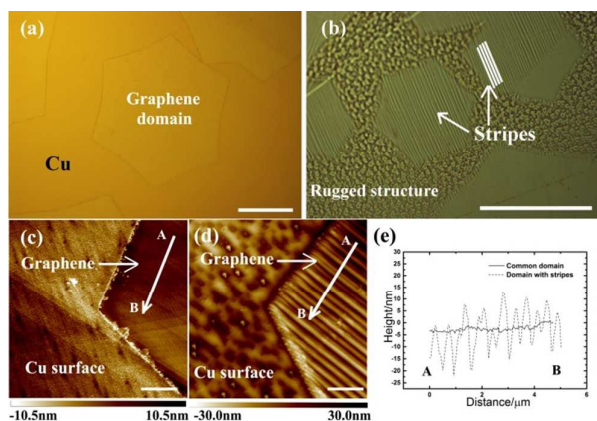


Fig 1. Optical images of (a) common hexagonal single-crystal domains and (b) those with parallel stripes. Scale bar: 50 μm . (c-d) AFM images show one corner of the hexagonal domains. Scale bar: 2 μm . (e) The corresponding line profile taken along the A–B arrow in (c) and (d).

because of their size (in nanometers). A previous study used hydrogen etching to conveniently detect the distribution and morphology of wrinkles in graphene²⁷. In that work, numerous trenches were observed on the initial graphene domains after etching. They proved that the trenches were bound with the formed wrinkles. In this work, graphene domains with parallel stripes are etched by hydrogen and the result reveals that the stripes suppress the formation of wrinkles along the stripes' direction. The distribution of Cu grains and the cooling rate during CVD mainly influences the stripe formation. Importantly, the sheet resistances of continuous graphene films are reduced by enlarging the coverage area of the stripe. The stripes help to release the internal strain between graphene and the Cu substrate, thereby contributing to the low wrinkle density in graphene.

Results and discussion

Hexagonal single-crystal graphene domains were synthesized (Figure 1a). Parallel stripes form on some of the hexagonal domains (see Figure 1b; the rugged Cu surface will be discussed later). The AFM results indicate that graphene domains with parallel stripes exhibit different surface morphology (Figure 1c: one corner of the hexagonal domain with stripes; and Figure 1d: common graphene domain). The common graphene surface is flat but the stripes (we call them CSR stripes) area is undulate. The stripes cover the whole graphene domain with their heights ranging from 5 nm to 100 nm (see Figure S1a and S1b). Even though these stripes were previously observed^{28, 29}, the height range in this study is 100 times higher than those in those published work²⁴.

The CSR stripes are associated with graphene wrinkles. The wrinkle distribution difference was revealed by hydrogen etching. The graphene domains were etched with hydrogen at 900 °C for 30 min. After the wrinkles areas were destroyed, etched trenches formed at the wrinkles position (Figure 2a). The trenches are either reticulate or approximately parallel

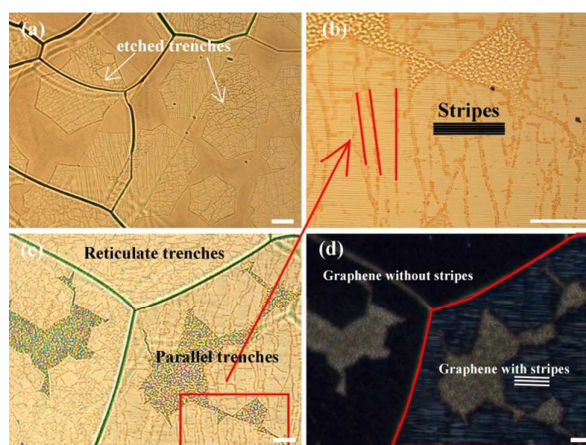


Fig 2. (a) Optical images of the trenches distribution after graphene domains were etched by hydrogen. (b) Magnified image of the rectangular area in the distribution of etched trenches that are always perpendicular to the stripes. (c) Distribution of etched trenches. (d) Dark-field image of the graphene domains to illustrate the CSR area, which is the same region in (c). Scale bar: 50 μm

(Figure 2b, the magnified image of a selected area in Figure 2c). The CSR area (the area full of parallel CSR stripes) can easily be discerned in a dark-field image because dark-field images provides an enhanced contrast to detect the graphene morphology and surface undulation²⁹. According to Figures 2c and 2d, reticulate trenches are observed on common graphene (the upper left corner in Figures 2c and 2d) but the trenches are approximately parallel on the CSR area and perpendicular to the CSR stripes (the lower right corner). More evidences are provided in Figures S2a to S2d.

Further observation of the relationship between graphene wrinkles and CSR stripes is investigated on hexagonal single-crystal domains. Hexagonal graphene domains in Figures 3a and 3b are obtained at the different position of one sample

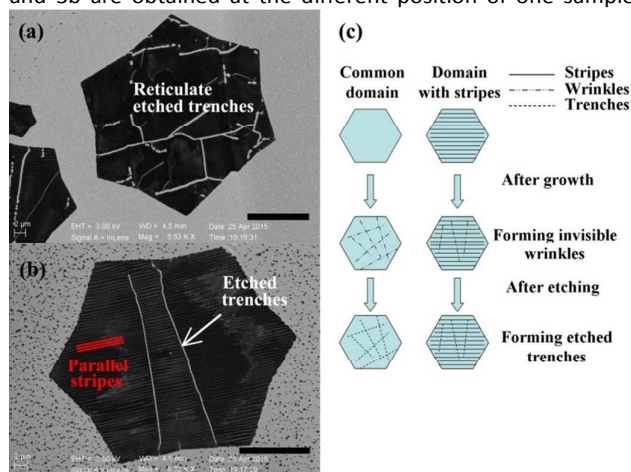


Fig 3. SEM images show (a) reticulate etched trenches on common hexagonal single-crystal domains and (b) the approximately parallel etched trenches on graphene with CSR stripes. Scale bar: 10 μm . (c) Schematic diagram reveals reticulate and parallel etched trenches formation.

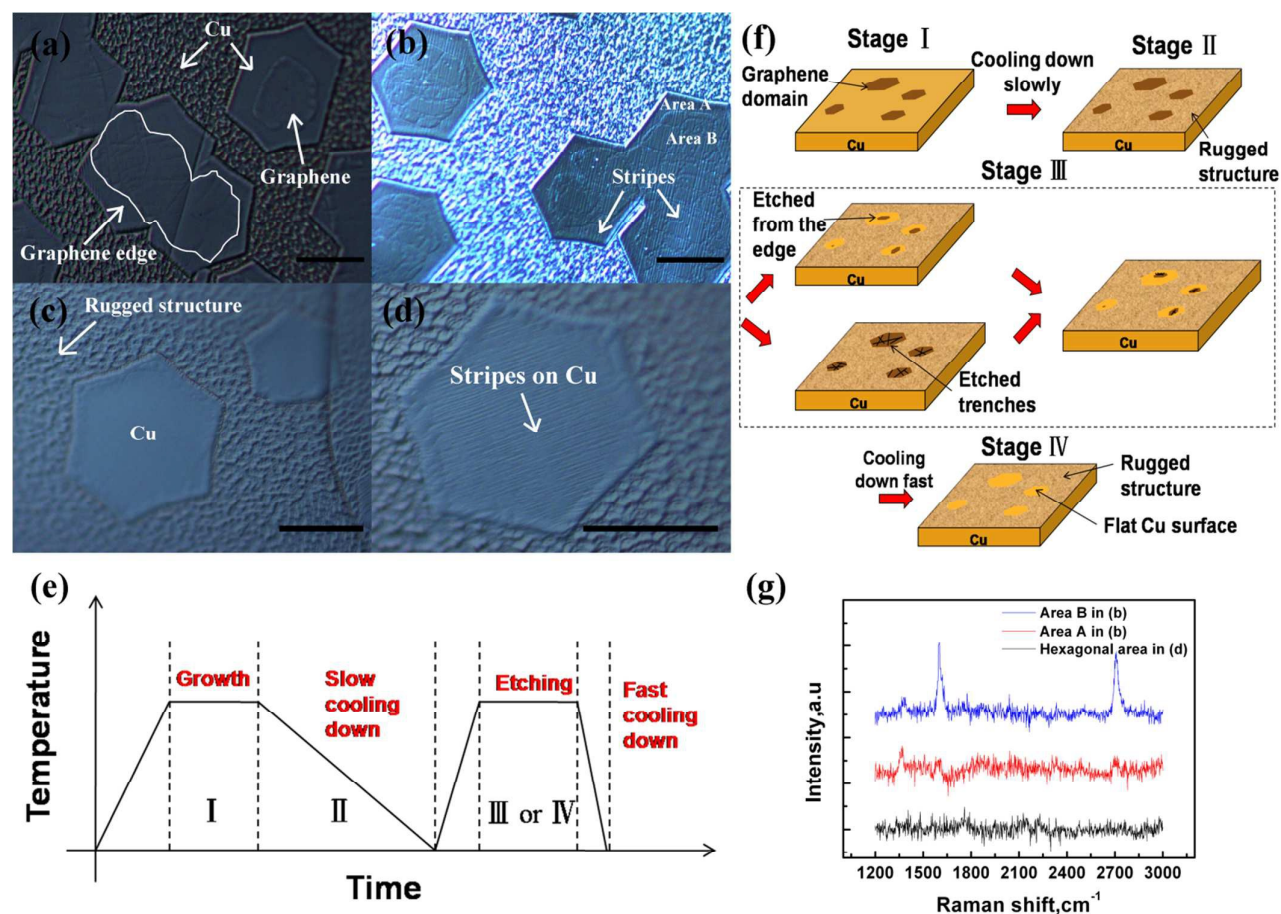


Fig 4. Images of the partially etched domains (a) without and (b) with stripes; fully etched domains (c) without and (d) with stripes. (e) Schematic of the etching process. (f) The formation of hexagonal Cu areas. (g) Raman results of the hexagonal areas of (b) and (d). Scale bar: 25 μm .

(both the domains were synthesized and etched in the same growth and etching condition). The common graphene domain exhibits reticulate etched trenches (Figure 3a) while graphene domain with CSR stripes shows approximately parallel etched trenches (perpendicular to the CSR stripes; Figure 3b). Graphene domain with CSR stripes displays lower etched trenches density than common domain, suggesting a lower graphene wrinkle density. Figure 3c illustrates the difference between common and CSR area domains. Wrinkle areas can be easily destroyed by etching, leaving the etched trenches which represent the wrinkle distribution on graphene^{23, 27}; Mismatches of the thermal expansion coefficients between graphene and its substrate contribute to the internal stress of graphene, which will result in anisotropic graphene wrinkles formation²⁵. Reticular etched trenches in the common hexagonal single-crystal domains suggest the anisotropic wrinkles or wrinkle-dependent defects. However, the trenches are approximately parallel and perpendicular to the CSR stripes, meaning that the graphene wrinkles are perpendicular to CSR stripes. CSR deformation only happens in the perpendicular direction to wrinkles, suggesting the CSR stripes formation facilitate the release of the perpendicularly internal stress. The Cu surface is prone to deformation for temperatures near the melting point. In addition, graphene

coatings could influence the deformation by limiting Cu sublimation and atom migration. The parallel stripes are formed when the graphene-coated surface shrunk during cooling. The internal stress is released by the production of undulate contracture, especially in the direction perpendicular to the stripes. Hence, the formation of wrinkles in this direction is avoided.

The CSR stripes are formed during cooling^{24, 30}. However, information about their formation remains few. Our results imply that the CSR stripes are comprised by reconstructed regular Cu. The graphene domains on the Cu-reconstructed area were etched by introducing hydrogen gas at 1050°C for 5 min. The results show that both the common and CSR area domains are etched from the edge to the center with few graphene residues (Figures 4a and 4b). The etched trenches are spread on the graphene surface, but are reduced upon approaching the hexagon edge. The partially etched domains (Figures 4a and 4b) were then transferred on the SiO₂/Si substrate (Figure S3). Raman tests were used to distinguish between graphene and Cu. The results verify that the hexagonal regions are Cu (Figure 4g; transferred samples are shown in Figure S3d). Figures 4c and 4d indicate that graphene are completely etched where hexagonal Cu regions are formed. In the CSR area, the stripes are observed on the hexagonal Cu

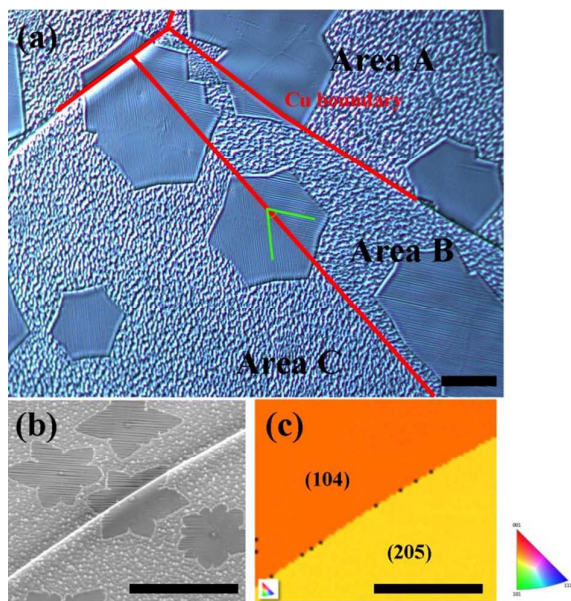


Fig 5. (a) Image of the stripes on graphene domains for different Cu grains. (b) CSR stripes that are cut off by the Cu boundary. (c) EBSD results showing Cu grain facet index in the same region as (b). Scale bar: 25 μm .

regions (Figure 4d). The absence of graphene suggests the stripes are the reconstructed Cu. The differences in hexagonal Cu regions and the external rough and rugged surface are caused by different cooling rates (as Figure 4f shown). We find samples experienced fast cooling result in flat surface (Figure S4a) while the ones experienced slow cooling exhibits rugged surface (Figure S4b). The rugged surface is covered with dendrite-like structures (see Figure S4c and S4d). The dendrite-like structures may cause by small perturbation in the course of solidification due to the thermal quenching on the unstable solid-melt interface at such high temperature³¹. The whole etching process can be concluded as follows. First, graphene domains were prepared (stage I, Figures 4e and 4f). Slow cooling was then introduced after these domains were synthesized. The Cu surface was highly damaged, resulting in a rugged construction (stage II, Figures 4e and 4f)³¹. The graphene-coated Cu was protected, and the flat hexagonal Cu regions were maintained until the graphene domains were etched. Graphene was then etched from the edges and the wrinkles area, which yielded irregular graphene edges and etched trenches (stage III, Figure 4f). Finally, the graphene domains were rapidly cooled to inhibit the rugged construction (stage IV, Figure 4f). Thus, the new exposed Cu surface was kept flat where graphene was etched away.

The growth of graphene is markedly influenced by Cu substrates pretreatment^{32, 33} and the crystallographic orientation^{34, 35}. The substrate surface affects the distribution of CSR stripes. Figure 5a illustrates the hexagonal single-crystal graphene domains separated by a Cu line boundary with two types of stripes at different directions (areas B and C). The stripes are always parallel in the same Cu grain regardless of the graphene domains (area B); some Cu grains are unsuitable for stripe formation (area A). The electron back-scattered

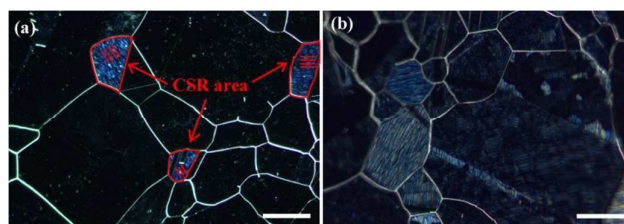


Fig 6. Dark-field images of CSR on graphene films at (a) approximately 200 $^{\circ}\text{C}/\text{min}$ and (b) 2 $^{\circ}\text{C}/\text{min}$. Scale bar: 200 μm .

diffraction (EBSD) was applied for flower-like graphene domains to determine the types of Cu grains which can form CSR stripes (Figures 5b and 5c). Clear images of CSR stripes are obtained on Cu grains [e.g., Cu (104)]. Different Cu orientations possess different surface energy, resulting in different Cu surface atom migration ability and restructure possibility. When the sample was cooled down, the differences in thermal expansion and Cu surface-graphene reaction shrunk graphene and Cu, thereby produce wrinkles. The formation of CSR stripes is another way to release the internal stress in graphene. The formation of wrinkles and CSR stripes are competing. Graphene wrinkles can cause relatively low transport mobility in CVD graphene and they are hard to remove. However, CSR stripes formation can be controlled because it is substrate-dependent different from the wrinkles. We can promote CSR stripes formation thereby limiting wrinkle density in graphene films.

Different cooling rates during CVD were used to analyze the formation of CSR stripes. These stripes do not run through the whole grain (Figures S6a and S6b) during slow cooling; this result is not mentioned in other studies. Partial CSR stripes occurred in one graphene domain. EBSD tests prove that this graphene domain with partial CSR stripes were located in one Cu grain (Figure S7). Partial stripes are formed in Cu grains where CSR is easily formed, and the slow cooling rate provided enough time for the surface to shrink and form stripes. The cooling rate is another important factor aside from the Cu grain crystallographic orientation. Fast cooling processes created small-area CSR (Figure 6a); hence, the CSR coverage increases in the continuous graphene film via slow cooling (Figure 6b).

Four samples were prepared to verify the effects of cooling rate on the properties of the continuous graphene films that were synthesized in the same CVD growth condition but different cooling rates. Samples A and B were synthesized at a slow cooling rate (about 2 $^{\circ}\text{C}/\text{min}$) to increase the CSR area, whereas the other samples were rapidly cooled at approximately 200 $^{\circ}\text{C}/\text{min}$. Samples A and B exhibit higher CSR coverage areas than samples C and D (Table 1).

Table 1. CSR area coverage and the average sheet resistance for continuous graphene films at various cooling rates

Sample	Cooling rate ($^{\circ}\text{C}/\text{min}$)	CSR area coverage (%)	Average sheet resistance (Ω)
A	~ 2	76	578.9
B	~ 2	71	698.2
C	~ 200	15	964.1
D	~ 200	17	817.4

All the continuous graphene film samples were transferred on the SiO₂/Si substrate for electrical properties testing. Results show the CSR coverage area and the sheet resistance are markedly correlated (tested by the four-point probe tester, RTS-9). The tests were repeated several times on different areas of each sample to reduce the test error. Samples A and B exhibit lower average sheet resistances (approximately 550-700 Ω) than samples C and D (approximately 800-1000 Ω). CSR stripes improve the electrical properties of graphene by releasing internal stress and reducing wrinkles. The resistance of the graphene film can be reduced by increasing the CSR area. Our etching work suggests that the CSR area contains a few wrinkles because the stripe formation reduces the internal stress and the number of wrinkles in the film. Hence, the sheet resistance is decreasing.

Conclusions

Cu stripes in graphene domains were verified by experimental analyses. The stripes bound to the etched trenches indicated the distribution of wrinkles in graphene, based on the results of thermal hydrogen etching. The stripes originated from Cu reconstruction and were affected by the distribution of Cu grains and cooling rate after the growth period. The stripes reduce the internal stress of graphene and the wrinkle density. The resistance of the graphene films can be reduced by increasing CSR area.

Experimental

Graphene was synthesized on Cu foils (purity, 99.8%; thickness, 100 μm) in a horizontal quartz tube furnace via atmospheric pressure chemical vapor deposition. The samples were then annealed for 1 h under Ar/H₂ flow (ratio, 5:1) at 1050 °C prior to graphene growth to remove surface contamination and increase the size of Cu grains. Then argon, hydrogen and argon diluted methane (CH₄/Ar = 0.5:100) gases were fed at different flow rates into the reaction chamber at 1050 °C. The graphene domains were synthesized for 30 min at gases ratio of 1000: 20: 1.5 and the graphene continuous film were synthesized in two steps (step one, 1000: 20: 1.5 for 60min; and step two, 1000: 20: 10 for 30min). Upon graphene synthesis, the samples were cooled down to room temperature at different cooling rates. Hydrogen etching was performed to detect the distribution and morphology of wrinkles. The graphene/Cu samples were placed in the quartz tube furnace. Thermal hydrogen etching was performed on these samples using Ar (1000 sccm) and H₂ (200 sccm) flow at atmospheric pressure. Etching was performed at 900 or 1050 °C for 30 min for different samples.

Acknowledgements

This work was supported the by National Science and Technology Major Project (Grant No. 2011ZX02707), the

National Natural Science Foundation of China (Grant No. 61136005), Chinese Academy of Sciences (Grant No. KGZD-EW-303), and the government of Shanghai (Grant Nos. 12JC1403900 and 12JC1410100).

Notes and references

1. A. K. Geim and K. S. Novoselov, *Nat Mater*, 2007, **6**, 183-191.
2. X. S. Li, W. W. Cai, J. H. An, S. Kim, J. Nah, D. X. Yang, R. Piner, A. Velamakanni, I. Jung, E. Tutuc, S. K. Banerjee, L. Colombo and R. S. Ruoff, *Science*, 2009, **324**, 1312-1314.
3. W. Liu, H. Li, C. Xu, Y. Khatami and K. Banerjee, *Carbon*, 2011, **49**, 4122-4130.
4. X. S. Li, C. W. Magnuson, A. Venugopal, R. M. Tromp, J. B. Hannon, E. M. Vogel, L. Colombo and R. S. Ruoff, *J Am Chem Soc*, 2011, **133**, 2816-2819.
5. S. Bhaviripudi, X. T. Jia, M. S. Dresselhaus and J. Kong, *Nano Lett*, 2010, **10**, 4128-4133.
6. K. Celebi, M. T. Cole, K. B. K. Teo and H. G. Park, *Electrochem Solid St*, 2012, **15**, K1-K4.
7. C. Hwang, K. Yoo, S. J. Kim, E. K. Seo, H. Yu and L. P. Biro, *J Phys Chem C*, 2011, **115**, 22369-22374.
8. I. Vlassiok, M. Regmi, P. F. Fulvio, S. Dai, P. Datskos, G. Eres and S. Smirnov, *Acs Nano*, 2011, **5**, 6069-6076.
9. A. W. Robertson and J. H. Warner, *Nano Lett*, 2011, **11**, 1182-1189.
10. E. Meca, J. Lowengrub, H. Kim, C. Mattevi and V. B. Shenoy, *Nano Lett*, 2013, **13**, 5692-5697.
11. B. Wu, D. C. Geng, Z. P. Xu, Y. L. Guo, L. P. Huang, Y. Z. Xue, J. Y. Chen, G. Yu and Y. Q. Liu, *Npg Asia Mater*, 2013, **5**.
12. H. S. Song, S. L. Li, H. Miyazaki, S. Sato, K. Hayashi, A. Yamada, N. Yokoyama and K. Tsukagoshi, *Sci Rep-Uk*, 2012, **2**.
13. L. P. Biro and P. Lambin, *New J Phys*, 2013, **15**.
14. F. Banhart, J. Kotakoski and A. V. Krasheninnikov, *Acs Nano*, 2011, **5**, 26-41.
15. W. J. Zhu, T. Low, V. Perebeinos, A. A. Bol, Y. Zhu, H. G. Yan, J. Tersoff and P. Avouris, *Nano Lett*, 2012, **12**, 3431-3436.
16. S. S. Chen, H. X. Ji, H. Chou, Q. Y. Li, H. Y. Li, J. W. Suk, R. Piner, L. Liao, W. W. Cai and R. S. Ruoff, *Adv Mater*, 2013, **25**, 2062-2065.
17. Y. F. Hao, M. S. Bharathi, L. Wang, Y. Y. Liu, H. Chen, S. Nie, X. H. Wang, H. Chou, C. Tan, B. Fallahzad, H. Ramanarayan, C. W. Magnuson, E. Tutuc, B. I. Yakobson, K. F. McCarty, Y. W. Zhang, P. Kim, J. Hone, L. Colombo and R. S. Ruoff, *Science*, 2013, **342**, 720-723.
18. T. R. Wu, G. Q. Ding, H. L. Shen, H. M. Wang, L. Sun, D. Jiang, X. M. Xie and M. H. Jiang, *Adv Funct Mater*, 2013, **23**, 198-203.
19. E. G. Steward, B. P. Cook and E. A. Kellett, *Nature*, 1960, **187**, 1015-1016.
20. K. V. Zakharchenko, M. I. Katsnelson and A. Fasolino, *Phys Rev Lett*, 2009, **102**.
21. D. Yoon, Y. W. Son and H. Cheong, *Nano Lett*, 2011, **11**, 3227-3231.
22. Y. F. Zhang, T. Gao, Y. B. Gao, S. B. Xie, Q. Q. Ji, K. Yan, H. L. Peng and Z. F. Liu, *Acs Nano*, 2011, **5**, 4014-4022.

ARTICLE

Journal Name

23. Y. H. Zhang, B. Wang, H. R. Zhang, Z. Y. Chen, Y. Zhang, Q. B. Wang, Y. P. Sui, X. L. Li, X. M. Xie, G. H. Yu, Z. Jin and X. Y. Liu, *Carbon*, 2014, **70**, 80-86.
24. J. F. Tian, H. L. Cao, W. Wu, Q. K. Yu, N. P. Guisinger and Y. P. Chen, *Nano Lett*, 2012, **12**, 3893-3899.
25. L. Meng, Y. Su, D. C. Geng, G. Yu, Y. Q. Liu, R. F. Dou, J. C. Nie and L. He, *Appl Phys Lett*, 2013, **103**.
26. C. F. Guo, V. Nayyar, Z. W. Zhang, Y. Chen, J. J. Miao, R. Huang and Q. Liu, *Adv Mater*, 2012, **24**, 3010-3014.
27. B. Wang, Y. H. Zhang, H. R. Zhang, Z. Y. Chen, X. M. Xie, Y. P. Sui, X. L. Li, G. H. Yu, L. Z. Hu, Z. Jin and X. Y. Liu, *Carbon*, 2014, **70**, 75-80.
28. K. Hayashi, S. Sato and N. Yokoyama, *Nanotechnology*, 2013, **24**.
29. X. H. Kong, H. X. Ji, R. D. Piner, H. F. Li, C. W. Magnuson, C. Tan, A. Ismach, H. Chou and R. S. Ruoff, *Appl Phys Lett*, 2013, **103**.
30. G. H. Han, F. Gunes, J. J. Bae, E. S. Kim, S. J. Chae, H. J. Shin, J. Y. Choi, D. Pribat and Y. H. Lee, *Nano Lett*, 2011, **11**, 4144-4148.
31. T. M. Paronyan, E. M. Pigos, G. G. Chen and A. R. Harutyunyan, *Acs Nano*, 2011, **5**, 9619-9627.
32. J. D. Wood, S. W. Schmucker, A. S. Lyons, E. Pop and J. W. Lyding, *Nano Lett*, 2011, **11**, 4547-4554.
33. W. H. Zhang, P. Wu, Z. Y. Li and J. L. Yang, *J Phys Chem C*, 2011, **115**, 17782-17787.
34. M. Ishihara, Y. Koga, J. Kim, K. Tsugawa and M. Hasegawa, *Mater Lett*, 2011, **65**, 2864-2867.
35. L. Zhao, K. T. Rim, H. Zhou, R. He, T. F. Heinz, A. Pinczuk, G. W. Flynn and A. N. Pasupathy, *Solid State Commun*, 2011, **151**, 509-513.